Bioorganic & Medicinal Chemistry 24 (2016) 2251–2256

Contents lists available at ScienceDirect

Bioorganic & Medicinal Chemistry

journal homepage: www.elsevier.com/locate/bmc

Development of ^{99m}Tc-labeled asymmetric urea derivatives that target prostate-specific membrane antigen for single-photon emission computed tomography imaging

Hiroyuki Kimura [a,b], Sotaro Sampei [a,†], Daiko Matsuoka [a], Naoya Harada [a], Hiroyuki Watanabe [a], Kenji Arimitsu [c], Masahiro Ono [a], Hideo Saji [a,*]

[a] Department of Patho-Functional Bioanalysis, Graduate School of Pharmaceutical Sciences, 46-29, Yoshida Shimoadachi-cho, Sakyo-ku, Kyoto 606-8501, Japan
[b] Department of Analytical and Bioinorganic Chemistry, Kyoto Pharmaceutical University, 5 Nakauchi-cho, Misasagi, Yamashina-ku, Kyoto 607-8414, Japan
[c] School of Pharmacy and Pharmaceutical Sciences, Mukogawa Women's University, 11-68 Koshien Kyuban-cho, Nishinomiya, Hyogo 663-8179, Japan

ARTICLE INFO

Article history:
Received 19 February 2016
Accepted 29 March 2016
Available online 30 March 2016

Keywords:
Prostate-specific membrane antigen
Single-photon emission computed tomography
Anionic ^{99m}Tc-tricarbonyl complex

ABSTRACT

Prostate-specific membrane antigen (PSMA) is expressed strongly in prostate cancers and is, therefore, an attractive diagnostic and radioimmunotherapeutic target. In contrast to previous reports of PMSA-targeting ^{99m}Tc-tricarbonyl complexes that are cationic or lack a charge, no anionic ^{99m}Tc-tricarbonyl complexes have been reported. Notably, the hydrophilicity conferred by both cationic and anionic charges leads to rapid hepatobiliary clearance, whereas an anionic charge might better enhance renal clearance relative to a cationic charge. Therefore, an improvement in rapid clearance would be expected with either cationic or anionic charges, particularly anionic charges. In this study, we designed and synthesized a novel anionic ^{99m}Tc-tricarbonyl complex ([^{99m}Tc]TMCE) and evaluated its use as a single-photon emission computed tomography (SPECT) imaging probe for PSMA detection. Direct synthesis of [^{99m}Tc]TMCE from dimethyl iminodiacetate, which contains both the asymmetric urea and succinimidyl moiety important for PSMA binding, was performed using our microwave-assisted one-pot procedure. The chelate formation was successfully achieved even though the precursor included a complicated bioactive moiety. The radiochemical yield of [^{99m}Tc]TMCE was 12–17%, with a radiochemical purity greater than 98% after HPLC purification. [^{99m}Tc]TMCE showed high affinity in vitro, with high accumulation in LNCaP tumors and low hepatic retention in biodistribution and SPECT/CT studies. These findings warrant further evaluation of [^{99m}Tc]TMCE as an imaging agent and support the benefit of this strategy for the design of other PSMA imaging probes.

1. Introduction

Prostate cancer is the most common malignancy in men in Europe and the United States.[1] Although prostate-specific antigen (PSA), a serum marker of prostate cancer, is useful for the early diagnosis of prostate cancer,[2] PSA levels provide no information about the location, progression, and spread of prostate cancer. At present, diagnostic imaging technologies, such as magnetic resonance imaging (MRI), computed tomography (CT), positron emission tomography (PET), and single-photon emission computed tomography (SPECT), are used to detect primary and metastatic prostate cancer. In particular, imaging is clinically important for prostate cancer detection, staging, prognosis, and post-therapy monitoring.

Prostate-specific membrane antigen (PSMA), which is abundantly expressed in prostate cancer, is an attractive diagnostic and radioimmunotherapeutic target.[3,4] Although PSMA is expressed in the normal prostate tissue, as well as in primary prostate cancer and lymph node metastases of prostate cancer,[3] PSMA expression 10- to 100-fold higher in prostate cancer than in normal prostate tissue.[5] Because PSMA is a membrane-anchored protein, the locations of metastases of prostate cancer can be diagnosed by PSMA imaging. Moreover, PSMA expression is upregulated in patients with hormone-refractory prostate cancer.[6]

PSMA is homologous to glutamate carboxypeptidase-II,[7–9] and asymmetric urea compounds (X-CO-Glu; X represents the amino acid) have been reported as glutamate carboxypeptidase-II (GCP-II) inhibitors.[10] We previously reported a drug design strategy for

* Corresponding author. Tel.: +81 75 753 4566; fax: +81 75 753 4568.
E-mail address: hsaji@pharm.kyoto-u.ac.jp (H. Saji).
† Contributed equally to this work.

http://dx.doi.org/10.1016/j.bmc.2016.03.051
0968-0896/

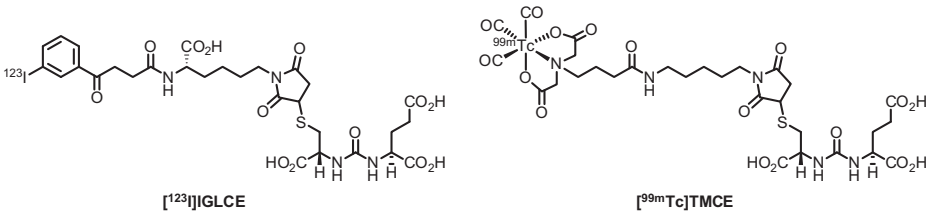

Figure 1. Chemical structures of [^{123}I]IGLCE and [^{99m}Tc]TMCE.

single-photon emission computed tomography (SPECT) using a nucleophilic conjugate addition between maleimide-based reagents and the thiol group of (*S*)-2-[3-[(*R*)-1-carboxy-2-mercaptoethyl]ureido-pentanedioic acid (Cys-CO-Glu)].[11] In that report, we additionally identified a succinimidyl moiety as an important PSMA-binding moiety, and prepared a novel PSMA-targeting agent ([^{123}I]IGLCE; Fig. 1).[11] However, [^{123}I]IGLCE exhibited high hepatic uptake and slow gastrointestinal clearance, characteristics that would contraindicate the use of this agent for prostate cancer imaging as prostate cancer most often metastasizes to the lower spine, pelvis, and lymph nodes within the abdominal cavity. Therefore, we concluded that decreased lipophilicity would be required to develop more useful PSMA imaging probes.

Technetium-99m (^{99m}Tc) is the most frequently used nuclide for SPECT imaging because it possesses radiochemical characteristics such as a suitable gamma emission energy level (141 keV) and adequate half-life (6.01 h). In addition, ^{99m}Tc is easily prepared using a ^{99}Mo–^{99m}Tc generator, which yields the ^{99m}Tc-containing molecule Na^{99m}TcO$_4$. Monovalent ^{99m}Tc-tricarbonyl complexes are expected to be available in the field of radiopharmaceuticals because of their compact structure, which allows linkages with low-molecular-weight bioactive ligands that have little influence on physiological activities and stability in a living body.[12,13] These factors led to our decision to use ^{99m}Tc-tricarbonyl complexes in this study.

Previous reports have described several ^{99m}Tc-tricarbonyl PSMA-targeting agents,[14–16] and suggested that higher hydrophilicity, in addition to high affinity, could lead to a lower uptake in non-target tissues, such as the liver, and high uptake in target tissues.[14,15] Although several PSMA-targeting ^{99m}Tc-tricarbonyl complexes were developed,[14–16] none of these agents have been anionic ^{99m}Tc-labeled complexes. Accordingly, we designed a novel anionic ^{99m}Tc-tricarbonyl complex ([^{99m}Tc]TMCE; Fig. 1) and evaluated its binding affinity for PSMA and biodistribution to confirm the importance of affinity, hydrophilicity, and electric charge in the pharmacokinetics of PSMA imaging probes.

2. Results and discussion

2.1. Drug design

We previously reported our work with the novel PSMA imaging probes, [^{123}I]IGLCE.[11] Because [^{123}I]IGLCE exhibited a high affinity for PSMA, we hypothesized the existence of interactions between [^{123}I]IGLCE and PSMA. We then identified a succinimidyl moiety as an important factor in this high-affinity interaction through structure–activity relationship and docking simulation studies. However, [^{123}I]IGLCE exhibited reduced tumor accumulation when compared to previously reported PSMA probes, such as [^{123}I]MIP-1072,[17,18] even though [^{123}I]IGLCE had higher affinity for PSMA than did [^{123}I]MIP-1072.[11]

We considered that this lower tumor accumulation might be attributable to the lower hydrophilicity of [^{123}I]IGLCE, as [^{123}I]IGLCE exhibited high hepatic uptake in a biodistribution study. High hepatic uptake likely led to rapid blood clearance and thus prevented PSMA imaging probes from migrating to tumors formed by LNCaP prostate adenocarcinoma cells. Therefore, we concluded that both high affinity and increased hydrophilicity should be conserved in order to improve tumor accumulation and reduce the hepatic uptake of [^{123}I]IGLCE. Therefore, we designed an anionic ^{99m}Tc-tricarbonyl complex with high hydrophilicity due to strong polarity and electric charges with the intent to further decrease non-target tissue uptake and enhance renal clearance.

2.2. Chemistry and radiochemistry

As shown in Scheme 1, the target asymmetric urea derivative **7**, a ^{99m}Tc-chelating precursor, was synthesized from a 4-aminobutanoic acid (**1**). After esterification of **1**, benzyl ester **2** was reacted with methyl bromoacetate to yield iminodiacetate **3**. Deprotection of the benzyl group in **3** and subsequent condensation with *N*-hydroxysuccinimide yielded active ester **5**. Subsequently, **5** was reacted with *N*-(5-aminopentyl)maleimide to result in amide **6**,

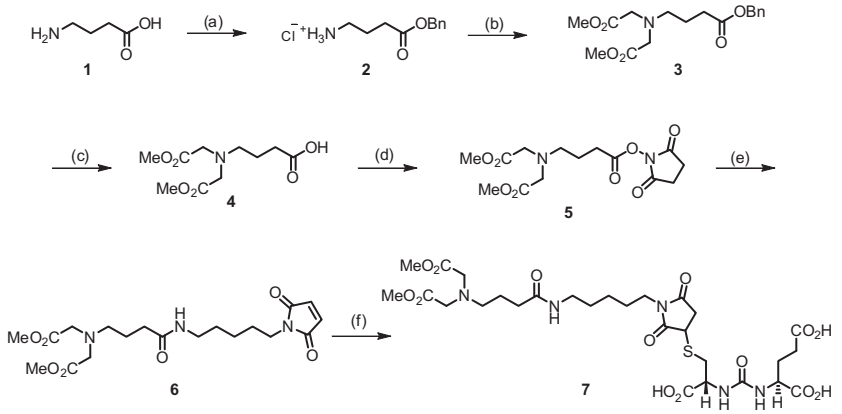

Scheme 1. Synthesis of precursor **7**. Reagents and conditions: (a) $SOCl_2$, benzyl alcohol, 87%; (b) $BrCH_2COOCH_3$, DMF, 57%; (c) Pd/C, under H_2, EtOAc, 85%; (d) NHS, WSCI, DMF, 57%; (e) *N*-(5-aminopentyl)maleimide hydrochloride, DIEA, CH_3CN, 90%; (f) Cys-CO-Glu, NaOH, H_2O, CH_3CN, 19%.

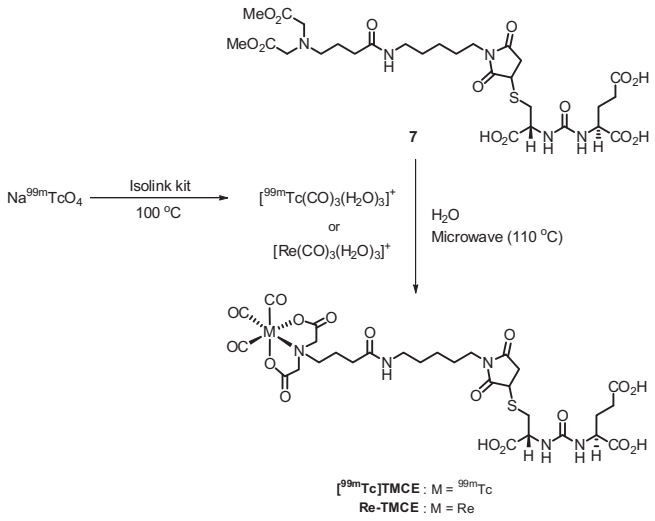

Scheme 2. Microwave-assisted synthesis of [^{99m}Tc]TMCE and Re-TMCE.

of which the maleimide moiety was found to be important for conjugation with asymmetric urea and high affinity for PSMA.[11] The conjugate addition of the thiol group from Cys-CO-Glu to the maleimide moiety in **6** formed the desired asymmetric urea derivative, **7**, as a chelating precursor.

[^{99m}Tc]TMCE was synthesized from precursor **7** and [^{99m}Tc$(CO)_3(H_2O)_3]^+$ using a previously described microwave-assisted one-pot procedure (Scheme 2).[19] Generally, ^{99m}Tc-labeled reactions cannot be performed using a conventional heating method such as oil bath heating because of precursor decomposition. Because our method does not incorporate conventional hydrolysis procedures or a long reaction process, we expected that it would eliminate decomposition of the bioactive ligand and subsequent decreases in chemical yield and reproducibility. Indeed, the reaction yielded [^{99m}Tc]TMCE with a radiochemical yield of 12–17% (calculated from $Na^{99m}TcO_4$). The radiochemical purity after HPLC purification was greater than 98%, and HPLC analysis of the purified [^{99m}Tc]TMCE showed a single peak (t_R: 26.5 min) that closely corresponded to Re-TMCE (t_R: 26.7 min), which was synthesized from $[Re(CO)_3(H_2O)_3]^+$ using a similar method. In summary, we succeeded in synthesizing a novel anionic ^{99m}Tc-tricarbonyl complex from a precursor with the complicated structure required for PSMA binding through a microwave-assisted one-pot synthesis procedure.

2.3. In vitro cell binding assay (selectivity and inhibition assays)

The uptake of [^{99m}Tc]TMCE into LNCaP cells was evaluated to clarify whether [^{99m}Tc]TMCE binds to membranous PSMA (see Fig. 2). This uptake was significantly inhibited by the GCP-II inhibitor, 2-PMPA. In addition, uptake into LNCaP cells was significantly higher than that into PC-3 prostate cancer cells, and uptake into the latter cells was non-significantly inhibited by 2-PMPA. These results indicate that uptake of [^{99m}Tc]TMCE into LNCaP cells only resulted from binding to PSMA.

To further evaluate the quantitative binding affinity of [^{99m}Tc]TMCE for PSMA, we performed an inhibition binding assay in LNCaP cells, using 2-PMPA as a competitive ligand. We evaluated the binding affinities of [^{99m}Tc]TMCE, [^{125}I]IGLCE, and [^{125}I]DCIT[21] for PSMA. The data (analyzed using Prism 5 software; GraphPad, Inc., San Diego, CA, USA) are shown in Figure 3. 2-PMPA competed with the uptake of all three PSMA-targeting probes into LNCaP cells, with 2-IC_{50} values of 3.4, 0.20, and 0.080 nM in the presence of [^{99m}Tc]TMCE, [^{125}I]IGLCE, and [^{125}I]DCIT, respectively. These

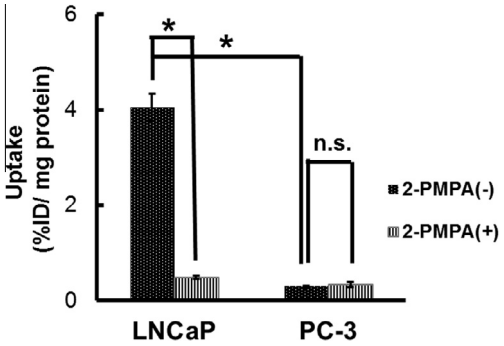

Figure 2. In vitro selectivity assay. The uptake of [^{99m}Tc]TMCE into each cell after incubation with or without 2-PMPA was evaluated; values are presented in units of % ID/mg protein. Uptake was significantly higher into LNCaP (PSMA-positive) cells than into PC-3 cells (PSMA-negative) and inhibited LNCaP cells ($n = 3$, $^*P < 0.05$).

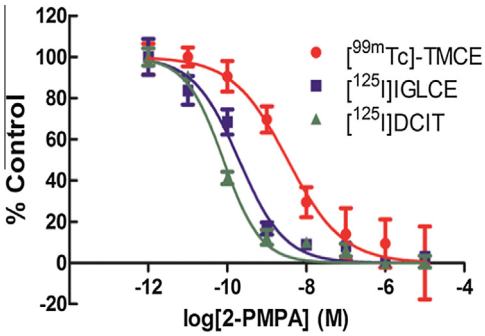

Figure 3. In vitro inhibition assay. Displacement curves of three radiolabeled probes, [^{99m}Tc]TMCE, [^{125}I]IGLCE, and [^{125}I]DCIT, in an inhibition assay based on the binding of 2-PMPA to PSMA. Values are shown as the means ± standard errors of three independent experiments.

results suggest that all three probes have a similarly high affinity for PSMA.

2.4. In vivo biodistribution and blocking studies

An in vivo biodistribution study of [^{99m}Tc]TMCE was performed using LNCaP tumor-bearing mouse models to confirm the viability of our design strategy. The biodistribution data of [^{99m}Tc]TMCE and the tumor-to-blood, -muscle, and -liver ratios are shown in Table 1.

Table 1
In vivo biodistribution of [^{99m}Tc]TMCE: Each mouse was sacrificed at 5 min, 30 min, or 2 h after injection. Accumulation in each tissue (except for stomach) was evaluated; all values are presented in units of % ID/g tissue. Accumulation in the stomach is presented in units of % ID/tissue. Values are expressed as means ± standard deviations. Ratios are based on the % ID/g tissue values

Tissues (% ID/g)	Time after injection		
	5	30	120
Blood	11.4 ± 2.3	3.2 ± 0.5	0.6 ± 0.1
Heart	4.1 ± 1.1	1.7 ± 0.4	0.2 ± 0.0
Lung	9.6 ± 1.2	3.0 ± 0.3	0.4 ± 0.0
Liver	5.7 ± 1.0	2.3 ± 0.3	1.1 ± 0.1
Kidney	124.9 ± 26.2	136.0 ± 6.4	56.8 ± 20.6
Stomach	1.1 ± 0.2	0.4 ± 0.2	0.1 ± 0.0
Intestine	3.3 ± 0.8	2.3 ± 0.2	1.7 ± 0.4
Spleen	15.9 ± 4.6	18.8 ± 4.6	4.9 ± 3.8
Pancreas	3.8 ± 1.0	1.5 ± 0.2	0.3 ± 0.1
Muscle	1.5 ± 0.5	1.0 ± 0.6	0.3 ± 0.1
LNCaP	4.0 ± 1.2	12.8 ± 2.2	5.0 ± 2.7
LNCaP/blood	0.4 ± 0.2	4.1 ± 1.3	9.3 ± 5.8
LNCaP/muscle	3.0 ± 1.5	16.8 ± 10.5	14.4 ± 2.7
LNCaP/liver	0.7 ± 0.3	5.6 ± 1.5	4.4 ± 2.4

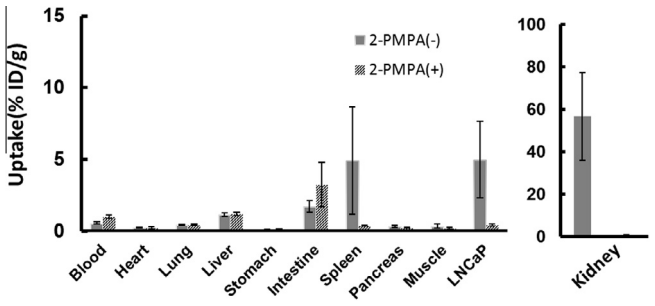

Figure 4. In vivo blocking study. All mice were sacrificed 2 h after injection. Accumulation in each tissue (except for stomach) was evaluated and is presented in units of % ID/g tissue. Accumulation in the stomach is presented as % ID/tissue.

[^{99m}Tc]TMCE exhibited good tumor uptake by LNCaP tumors (12.8% ID/g at 30 min), and this accumulation was maintained for at least 2 h. Because high uptake in LNCaP tumors was observed, a blocking study was performed to confirm whether this tumor uptake was due to PSMA-specific binding. Tumor uptake was significantly inhibited (0.10% ID/g at 2 h) following co-injection of the GCP-II inhibitor 2-PMPA (Fig. 4; $n = 3$, $^{*}P < 0.05$).

As expected, [^{99m}Tc]TMCE exhibited lower hepatic accumulation (1.1% ID/g at 2 h), when compared [^{123}I]IGLCE, and hepatic accumulation was not blocked in the blocking study, suggesting that the hepatic accumulation of [^{99m}Tc]TMCE was not due to PSMA-specific binding and that high hydrophilicity led to low hepatic accumulation. [^{99m}Tc]TMCE also displayed the expected enhanced hepatobiliary clearance. However, remarkably enhanced renal clearance was not observed, and the renal uptake of [^{99m}Tc]TMCE began to decrease at 2 h after injection.

In accordance with a previous study, higher uptake of ^{99m}Tc-MIP-1404, a cationic ^{99m}Tc-tricarbonyl complex, than of [^{99m}Tc]TMCE was observed in the LNCaP tumor xenograft, and the rate of uptake increased until 2 h after injection.[14] Moreover, the uptake of ^{99m}Tc-MIP-1404 in kidney only began to decrease at 4 h after injection, after maintenance for 2 h after injection.[14] On the other hand, [^{99m}Tc]**L8**, a ^{99m}Tc-tricarbonyl complex without a net charge, exhibited high tumor uptake, but slow hepatobiliary and renal clearance.[16] These results indicate that the hydrophilicity associated with both cationic and anionic charges leads to rapid hepatobiliary clearance and that anionic charges might enhance renal clearance to a greater extent than cationic charges. Therefore, more rapid clearance would be necessary for cationic or anionic charges, particularly anionic charges.

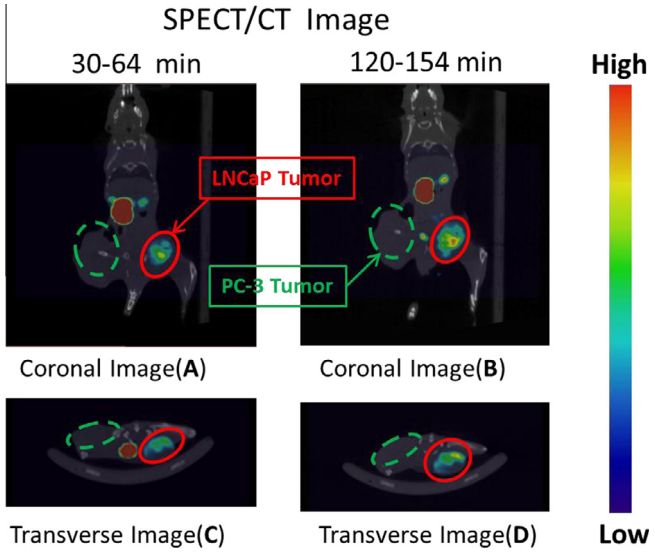

Figure 5. SPECT/CT images of [^{99m}Tc]TMCE. (A and B) coronal SPECT/CT images of [^{99m}Tc]TMCE distribution were obtained at 30 min (A) and 2 h (B) after injection. (C and D) transverse SPECT/CT images were obtained at 30 min (C) and 2 h (D) after injection. In all images, [^{99m}Tc]TMCE clearly illuminated LNCaP tumors (red arrow) but did not illuminate PC-3 tumors (green arrow).

2.5. SPECT study

A SPECT/CT study was performed on the basis of the biodistribution study results (see Fig. 5). SPECT scanning was initiated 30 min and 2 h after [^{99m}Tc]TMCE injection because the tumor uptake and tumor/blood ratio, respectively, were highest at these time points. [^{99m}Tc]TMCE clearly distinguished LNCaP tumors from PC-3 tumors on SPECT/CT images at both time points after injection. SPECT images additionally revealed that by 2 h postinjection, [^{99m}Tc]TMCE had been sufficiently excreted via the bladder to allow clear SPECT images. These results correlated well with those of the biodistribution study and suggested that [^{99m}Tc]TMCE would be an efficient PSMA imaging probe.

3. Conclusion

In this study, we designed and synthesized a novel ^{99m}Tc-labeled PSMA-targeting agent via microwave-assisted synthesis of [^{99m}Tc$(CO)_3(H_2O)_3]^+$ and dimethyl iminodiacetate derivative **7**, which was designed using [^{123}I]IGLCE as a model structure. Our microwave-assisted procedure was found to be applicable to ^{99m}Tc-complex formation using a complicated bioactive precursor such as the asymmetric urea **7**. [^{99m}Tc]TMCE exhibited high affinity for PSMA in vitro, as well as high accumulation in LNCaP tumors and low hepatic retention in the biodistribution and SPECT/CT studies. In this study, the hydrophilicity of both cationic and anionic charges led to rapid hepatobiliary clearance, although anionic charges might enhance renal clearance to a greater extent. These findings warrant the further evaluation of [^{99m}Tc]TMCE as an imaging agent and support the benefit of this strategy for the design of other PSMA imaging probes.

4. Experimental

4.1. General

W-Prep 2XY (Yamazen Corporation, Osaka, Japan) was used for silica gel column chromatography on a Hi Flash silica gel column (40 mm, 60 Å; Yamazen). Silica gel 60 F_{254} plates (0.5 mm; Merck KGaA, Darmstadt, Germany) were used for preparative thin layer chromatography (PTLC). An LC-20AD (Shimadzu Corporation, Kyoto, Japan) equipped with an SPD-20A UV detector (ρ; 220 and 254 nm; Shimadzu) and an NDW-351 radioisotope detector (Hitachi Aloka Medical, Ltd, Tokyo, Japan) was used for high-performance liquid chromatography (HPLC). The eluent comprised a binary mixture of 0.1% trifluoroacetic acid (TFA) in H_2O (solvent A) and 0.1% TFA in methanol (solvent B). Nanopure water was prepared with an MQ Integra15 (Nihon Millipore, Tokyo, Japan). Mass spectra were recorded on an LCMS-2010 EV (Shimadzu). ^{1}H NMR spectra were recorded on an LNM-AL500 (JEOL), using $CDCl_3$ or D_2O (Euriso-top, Saint-Aubin, France) as the solvent and tetramethylsilane or residual solvent as the internal standard. Microwave reactions were performed using a CEM Discover. All chemicals used in the syntheses were reagent grade. *N*-(5-Aminopentyl)-maleimide hydrochloride was synthesized according to previously reported methods.[11]

4.2. Animal experiments

Six-week-old male ddY mice were obtained from Japan SLC (Kyoto, Japan). C.B.-17/Icr +/+ Jcl mice and C.B.-17/Icr *scid*/*scid* Jcl mice were purchased from CLEA Japan (Tokyo, Japan). Animal studies were conducted in accordance with institutional guidelines, and the experimental procedures were approved by the Kyoto University Animal Care Committee.

4.3. Synthesis

4.3.1. 4-(Benzyloxy)-4-oxobutan-1-aminium chloride (2)

4-Aminobutanoic acid (1.03 g, 10 mmol) was added to benzyl alcohol (10 mL) on the ice. Thionyl chloride (1.1 mL, 1.5 mmol) was then added to the solution at 0 °C and stirred for 2 h at room temperature. After the solution changed to yellow, the solvent was evaporated and recrystallized to yield **2** (2.00 g, 87.0% yield), with the following characteristics: ^{1}H NMR (400 MHz, $CDCl_3$) δ: 8.23 (s, 3H), 7.25–7.37 (m, 5H), 5.07 (s, 2H), 3.09 (br, 2H), 2.50 (br, 2H), 2.10 (br, 2H); ESI-MS *m*/*z*: 194 $[M-Cl]^+$.

4.3.2. Benzyl 4-[bis(2-methyoxy-2-oxoethyl)amino]butanoate (3)

Methyl bromoacetate (0.42 mL, 4.5 mmol) was added to a solution of **2** (345 mg, 1.5 mmol) in DMF (3.5 mL). The reaction mixture was then stirred overnight at 80 °C, quenched with water, and extracted with EtOAc. The resultant extract was washed with brine and dried over Na_2SO_4. The solvent was removed using a rotary vacuum evaporator, and the residue was purified by silica gel chromatography (Hexane/EtOAc = 2:1) to yield **3** (289 mg, 57.0% yield) with the following characteristics: ^{1}H NMR (400 MHz, $CDCl_3$) δ: 7.35–7.36 (m, 5H), 5.11 (s, 2H), 3.69 (s, 6H), 3.53 (s, 4H), 2.75 (t, *J* = 6.96 Hz, 2H), 2.44 (t, *J* = 7.54, 2H), 1.77–1.84 (m, 2H); ESI-MS *m*/*z*: 338 $[M+H]^+$.

4.3.3. 4-[Bis(2-methoxy-2-oxoethyl)amino]butanoic acid (4)

Palladium on carbon (100 mg) was added to a solution of **3** (441 mg, 1.3 mmol) in EtOAc (5.0 mL). The reaction was stirred for 1 h under hydrogen atmosphere and filtered through celite, and the solvent was removed using a rotary vacuum evaporator to obtain **4** (274 mg, 85.3% yield), with the following characteristics: ^{1}H NMR (400 MHz, $CDCl_3$) δ: 3.72 (s, 6H), 3.58 (s, 4H), 2.82 (t, *J* = 6.38 Hz, 2H), 2.52 (t, *J* = 6.67 Hz, 2H), 1.77–1.84 (m, 2H); ESI-MS *m*/*z*: 248 $[M+H]^+$.

4.3.4. Succinimidyl 4-[bis(2-methoxy-2-oxoethyl)amino] butanoate (5)

N-Hydroxysuccinimide (380 mg, 3.3 mmol) and WSCI (630 mg, 3.3 mmol) were added to a solution of **4** (816 mg, 3.3 mmol) in DMF (10 mL). The reaction mixture was stirred overnight under an argon atmosphere at room temperature, quenched with saturated aqueous $NaHCO_3$, and extracted with EtOAc. The extract was washed with brine and dried over Na_2SO_4. The solvent was removed using a rotary vacuum evaporator, and the residue were purified via silica gel chromatography (Hexane/EtOAc = 1:1) to obtain **5** (646 mg, 56.9% yield). ESI-MS *m*/*z*: 345 $[M+H]^+$ and 343 $[M-H]^-$.

4.3.5. *N*-[5-(Maleimidyl)pentyl]-4-[bis(2-methoxy-2-oxoethyl) amino]butanamide (6)

To a solution of **5** (646 mg, 1.9 mmol) in MeCN (30 mL), *N*-(5-aminopentyl)maleimide hydrochloride (411 mg, 1.9 mmol) and DIEA (647 μL, 3.8 mmol) were added. After the reaction was stirred for 4 h, the reaction mixture was quenched with water and extracted with EtOAc. The extract was washed with brine and dried over Na_2SO_4. The solvent was removed under vacuum to yield **6** (695 mg, 89.8% yield). ^{1}H NMR (400 MHz, $CDCl_3$): δ 6.70 (s, 2H), 6.17 (s, 1H) 3.71 (s, 6H), 3.50–3.53 (m, 4H), 3.20 (dd, *J* = 6.96, 13.33 Hz, 2H), 2.73 (t, *J* = 6.38 Hz, 2H), 2.27 (t, *J* = 6.96 Hz, 2H), 1.75–1.81 (m, 2H), 1.57–1.64 (m, 4H), 1.48–1.56 (m, 2H), 1.24–1.34 (m, 2H); ESI-MS *m*/*z*: 412 $[M+H]^+$.

4.3.6. *N*-[(1*R*)-*N*-({2-[*N*-(5-{4-[Bis(2-methoxy-2-oxoethyl) amino]-1-oxobut-1-yl}amino)pentyl]succinimid-3-yl}thio)-1-carboxyethyl]carbamoyl-L-glutamic acid (7)

Product **6** (695 mg, 1.7 mmol) was added to a solution of Cys-CO-Glu (547.4 mg, 1.9 mmol) in aqueous MeCN (3.0 mL). The mixture was neutralized with 1 N NaOH and stirred overnight. Product **7** was purified by HPLC under the following conditions: YMC-Pack ODS-AQ 20-mm × 250-mm column, rate of 5 mL/min, solvent A/B gradient of 40/60 (0 min) to 90/10 (60 min), and 40–90% gradient of 0.1% TFA in methanol over 60 min (220.1 mg, 18.5% yield). The following characteristics were determined: ^{1}H NMR (400 MHz, D_2O): δ 4.45 (d, *J* = 4.58 Hz, 1H), 4.17–4.23 (m, 5H), 3.94–4.00 (m, 1H), 3.75 (s, 6H), 3.41 (t, *J* = 6.87 Hz, 2H), 3.31 (t, *J* = 7.16 Hz, 2H), 3.16–3.25 (m, 1H), 3.13 (t, *J* = 5.15 Hz, 1H), 3.07 (t, *J* = 6.87 Hz, 2H), 2.96–3.01 (m, 1H), 2.60 (dq, *J* = 18.90, 4.01 Hz, 1H), 2.42 (t, *J* = 7.16 Hz, 2H), 2.35 (t, *J* = 6.59 Hz, 2H), 2.09 (td, *J* = 13.60, 6.87 Hz, 1H), 1.84–1.96 (m, 3H), 1.85–1.88 (m, 3H), 1.38–1.50 (m, 4H), 1.14–1.20 (m, 2H); ESI-MS *m*/*z*: 706 $[M+H]^+$.

4.3.7. Re-TMCE

First, 50 μL of $[Re(CO)_3(H_2O)_3]^+$ were added to a solution of **7** (3.5 mg, 5.0 μmol) in water (450 μL); the resulting mixture was neutralized with 1 N NaOH and heated in a microwave reactor at 110 °C, 17 bars (max), and 300 W (max) for 5 min. Product **8** was purified by HPLC under the following conditions: $5C_{18}$-AR-II 4.6-mm × 150-mm column, rate of 1.0 ml/min, and solvent A/B gradient of 85/15 (0 min) to 20/80 (60 min). ESI-MS *m*/*z*: 945 $[M-H]^-$.

4.4. Radiosynthesis

In the present study, $[^{99m}Tc(CO)_3(H_2O)_3]^+$ was prepared as previously reported.[15] Briefly, $Na^{99m}TcO_4$ (37 MBq) solution was added to an IsoLink kit™ (Mallinckrodt Medical, Netherlands) and heated at 100 °C for 20 min.[19] First, 450 μL of $[^{99m}Tc(CO)_3(H_2O)_3]^+$ was added to 50 μL of a solution of **7** (1.0 mM) in water. Next, the mixture was neutralized with 3 N HCl and heated in a microwave reactor at 110 °C, 17 bar (max), and 300 W (max) for 5 min. Purification was conducted using preparative HPLC ($5C_{18}$-AR-II 4.6-mm × 150-mm column, rate of 1.0 ml/min, solvent A/B gradient of 85/15 (0 min) to 20/80 (60 min)). [^{99m}Tc]TMCE was obtained with a radiochemical yield of 14% (5.2 MBq, overall decay corrected) and the radiochemical purity of >98%.

4.5. Cell lines and mouse models

Two human prostate carcinoma cell lines were purchased from DS Pharma Biomedical (Osaka, Japan): LNCaP (PSMA-positive) and PC-3 (PSMA-negative).[6] The cells were cultured in Roswell Park Memorial Institute 1640 (RPMI 1640) medium supplemented with 10% fetal bovine serum, glutamine, and antibiotics (penicillin/streptomycin) in a humidified CO_2 incubator (37 °C/5% CO_2), as previously reported.[20]

Cultured cells were treated with 2.5 g/L trypsin/1 mM EDTA and re-suspended in phosphate-buffered saline. Subsequently, C.B.-17/Icr +/+ Jcl mice and C.B.-17/Icr *scid*/*scid* Jcl mice were each injected with 100 μL of a 1:1 mixture of cell suspension and BD Matrigel™ Basement Membrane Matrix ($1–5 \times 10^6$ cells/mouse) in the right (PC-3) or left (LNCaP) flank. Tumor-bearing mice were used for studies when tumors reached a diameter of approximately 10–15 mm.

4.6. In vitro cell binding assay (selectivity assay)

To confirm that [^{99m}Tc]TMCE binds selectively to PSMA, we performed cell uptake assays. LNCaP and PC-3 cells were incubated in 12-well plates (4×10^5 cells/well) for 48 h at 37 °C and 5% CO_2. The medium was removed, and each well was washed twice with 500 μL of assay medium (RPMI 1640 supplemented with 0.5% bovine serum albumin). Next, 500 μL of [^{99m}Tc]TMCE (final concentration, 74 kBq/mL) were added to each well, and the plates were incubated at 37 °C for 1 h. Nonspecific binding was evaluated by adding 1.0 mM 2-(phosphonomethyl)pentanedioic acid (2-PMPA), a GCP-II inhibitor. After incubation, each well was washed twice with 500 μL of fresh assay medium, and the cells were lysed with 0.2 N NaOH. Radioactivity bound to cells was measured with a γ-counter.

4.7. In vitro cell binding assay (inhibition assay)

The affinities of the novel compounds [^{125}I]IGLCE and [^{125}I]DCIT were determined through an in vitro inhibition binding assay, as previously reported.[11] Specifically, we compared the half-maximal inhibitory concentration (IC_{50}) values of [^{99m}Tc]TMCE with the above-mentioned compounds to confirm the high affinity of [^{99m}Tc]TMCE for PSMA. LNCaP cells were incubated in 12-well plates (4×10^5 cells/well) for 48 h at 37 °C and 5% CO_2. The medium was removed, and each well was washed twice with 500 μL of assay medium. Next, 500 μL of the radiolabeled compound ([^{99m}Tc]TMCE, [^{125}I]IGLCE, and [^{125}I]DCIT;[21] final concentration, 74 kBq/mL) and 2-PMPA (final concentration, 10 p–10 μM), a GCP-II inhibitor, were added to each well, and the plates were incubated at 37 °C for 1 h. After incubation, each well was washed twice with 500 μL of fresh assay medium, and the cells were lysed with 0.2 N NaOH. Radioactivity bound to cells was measured with a γ-counter. Finally, we calculated the IC_{50} values using GraphPad Prism 5.0.

4.8. In vivo biodistribution study

The distribution of [^{99m}Tc]TMCE in vivo was directly evaluated in model mice after determining a sufficiently high-affinity level. [^{99m}Tc]TMCE (100 μL) was injected via the tail vein into tumor-bearing mice weighing 20–24 g ($n = 3$ for each time point). Mice were sacrificed by decapitation at the following fixed time points post-injection: 5 min, 30 min, and 2 h. Tissue weights and radioactivity levels were measured, and [^{99m}Tc]TMCE uptake was evaluated as a percentage of the injected dose per gram of tissue (% ID/g).

4.9. In vivo blocking study

A blocking study was performed to confirm in vivo PSMA-specific binding. Briefly, 100 μL of [^{99m}Tc]TMCE were coinjected with 2-PMPA (10 mg/kg) into tumor bearing mice (weight 22–24 g) via the tail vein. Mice were decapitated 2 h after injection. Tissue weights and radioactivity levels were measured, and [^{99m}Tc]TMCE uptake was evaluated as% ID/g.

4.10. Small animal SPECT imaging

SPECT/CT studies were performed using a small animal scanner (FX3300 Imager; SII NanoTechnology Inc., Northridge, CA, USA). LNCaP and PC-3 tumor-bearing mice (20–25 g) were anesthetized with isoflurane (2.5% in an air mixture). Each mouse was injected with [^{99m}Tc]TMCE (9.45 MBq in 0.3 mL isotonic saline) via the tail vein. The mice were placed on a heating pad to maintain body temperature throughout the procedure.

SPECT scans were acquired over periods of 30–64 and 120–154 min after injection; CT scans were performed for anatomic reference (50 μm spatial resolution, 60 kV, and 310 μA). In the SPECT studies, all projection data were acquired using a 20% energy window centered at 140 keV for ^{99m}Tc, with a 35-mm radius of rotation, 360° circular orbit, 60-s projection time, and 32 projection angles. Single-pinhole collimators (1.0-mm diameter, 9.0-mm focal length) were used. SPECT images were reconstructed using three-dimensional ordered-subset expectation maximization, and CT images were reconstructed using a modified three-dimensional cone-beam Feldkamp algorithm resulting in a $0.177 \times 0.177 \times 0.177$ mm^3 voxel size for a $512 \times 512 \times 512$ image volume. Acquired SPECT and CT data sets were processed using AMIRA software (version 5.1; FEI Company, Hillsboro, Oregon, USA).

4.11. Statistical analysis

GraphPad Prism 5 software (GraphPad Software Inc., San Diego, CA, USA) was used for the statistical analyses. The Bonferroni multiple-comparison test was used to assess statistical differences in the biodistribution study. A P value of <0.05 was considered statistically significant.

Acknowledgments

This work was partly supported by the Practical Research for Innovative Cancer Control from the Japan Agency for Medical Research and Development (AMED), a Grant-in-Aid for Young Scientists (A) Grant Number 25713046 from the Japan Society for the Promotion of Science.

References and notes

1. Siegel, R.; Naishadham, D.; Jemal, A. *Ca–Cancer J. Clin.* **2013**, *63*, 11.
2. Hugosson, J.; Carlsson, S.; Aus, G.; Bergdahl, S.; Khatami, A.; Lodding, P.; Pihl, C.; Stranne, J.; Holmberg, E.; Lilja, H. *Lancet Oncol.* **2010**, *11*, 725.
3. Silver, D.; Pellicer, I.; Fair, W.; Heston, W.; CordonCardo, C. *Clin. Cancer Res.* **1997**, *3*, 81.
4. Lapidus, R.; Tiffany, C.; Isaacs, J.; Slusher, B. *Prostate* **2000**, *45*, 350.
5. Su, S.; Huang, I.; Fair, W.; Powell, C.; Heston, W. *Cancer Res.* **1995**, *55*, 1441.
6. Israeli, R.; Powell, C.; Fair, W.; Heston, W. *Cancer Res.* **1993**, *53*, 227.
7. Barinka, C.; Rojas, C.; Slusher, B.; Pomper, M. *Curr. Med. Chem.* **2012**, *19*, 856.
8. Carter, R.; Feldman, A.; Coyle, J. *Proc. Natl. Acad. Sci. U.S.A.* **1996**, *93*, 749.
9. Tiffany, C.; Lapidus, R.; Merion, A.; Calvin, D.; Slusher, B. *Prostate* **1999**, *39*, 28.
10. Kozikowski, A.; Nan, F.; Conti, P.; Zhang, J.; Ramadan, E.; Bzdega, T.; Wroblewska, B.; Neale, J.; Pshenichkin, S.; Wroblewski, J. *J. Med. Chem.* **2001**, *44*, 298.
11. Harada, N.; Kimura, H.; Ono, M.; Saji, H. *J. Med. Chem.* **2013**, *56*, 7890.
12. Albert, R.; Schibli, R.; Egli, A.; Schubiger, P. A.; Herrmann, W. A.; Artus, G.; Abram, U.; Kaden, T. A. *J. Organomett. Chem.* **1995**, *493*, 119.
13. Alberto, R.; Schibli, R.; Schubiger, A. P.; Abram, U.; Pietzsch, H.-J.; Johannsen, B. *J. Am. Chem. Soc.* **1999**, *121*, 6076.
14. Hillier, S. M.; Maresca, K. P.; Lu, G.; Merkin, R. D.; Marquis, J. C.; Zimmerman, C. N.; Eckelman, W. C.; Babich, J. W. *J. Nucl. Med.* **2013**, *54*, 1369.
15. Lu, G.; Maresca, K. P.; Hillier, S. M.; Zimmerman, C. N.; Eckelman, W. C.; Joyal, J. L.; Babich, J. W. *Bioorg. Med. Chem. Lett.* **2013**, *23*, 1557.
16. Banerjee, S. R.; Pullambhatla, M.; Foss, C. A.; Falk, A.; Byun, Y.; Nimmagadda, S.; Mease, R. C.; Pomper, M. G. *J. Med. Chem.* **2013**, *56*, 6108.
17. Hiller, S.; Maresca, K.; Femia, F.; Marquis, J.; Foss, C.; Nguyen, N.; Zimmerman, C.; Barrett, J.; Eckelman, W.; Pomper, M.; Joyal, J.; Babich, J. *Cancer Res.* **2009**, *69*, 6932.
18. Barret, J.; Coleman, R.; Goldsmith, S.; Vallabhajosula, S.; Petry, N.; Cho, S.; Armor, T.; Stubbs, J.; Maresca, K.; Stabin, M.; Joyal, J.; Eckelman, W.; Babich, J. *J. Nucl. Med.* **2013**, *54*, 380.
19. Kimura, H.; Mori, D.; Harada, N.; Ono, M.; Ohmomo, Y.; Kajimoto, T.; Kawashima, H.; Saji, H. *Chem. Pharm. Bull.* **2012**, *60*, 79.
20. Carter, R.; Feldman, A.; Coyle, J. *Proc. Natl. Acad. Sci. U.S.A.* **1996**, *93*, 749.
21. Foss, C.; Mease, R.; Fan, H.; Wang, Y.; Ravert, H.; Dannals, R.; Olszewski, R.; Heston, W.; Kozikowski, A.; Pomper, M. *Clin. Cancer Res.* **2005**, *11*, 4022.